Stiffness of the Extrafibrillar Phase in Staggered Biological Arrays

Benny Bar-On and H. Daniel Wagner*

Department of Materials and Interfaces, Weizmann Institute of Science, Rehovot 76100, Israel

(Received 17 April 2012; published 16 August 2012)

A number of important biological tissues such as nacre, tendon, and bone consist of staggered structural arrays as universal motifs. Such arrays usually include stiff fibril-like (or plateletlike, or needlelike) elements embedded in an extrafibrillar (XF) phase. This work discusses the effect of the stiffness of such an XF matrix on the elastic properties of the resulting staggered composite. In the case of most biological composites, this XF stiffness is hardly accessible and very little data are available. We develop an analysis based on previous analytical formulation that results in a relation between the XF modulus and the deformations of the staggered particles. This analysis is then used to back-calculate the yet unmeasured modulus of the XF phase from experimental deformation data, thereby providing a simple alternative to potentially complex direct measurements. This is demonstrated and validated for parallel-fiber bone tissue.

DOI: 10.1103/PhysRevLett.109.078102 PACS numbers: 87.10.Pq

Staggered structures typically include an array of discontinuous fibrils (or platelets, or needles) embedded in extrafibrillar (XF) matrix material. Such staggered structures are found in a variety of biological tissues such as nacre, tendon, bone, and more, and their mechanical characteristics depend on the geometry and the stiffness of their components. In nacre, the XF phase consists of organic material located between aragonite bricks. In tendon, it consists of noncollagenous material found between collagen fibrils. Bone is a more complex structure, because it includes several hierarchical scales. At the smaller scale of the single mineralized collagen fibril, the XF matrix is identified with the collagen medium located between staggered hydroxyapatite (HA) platelets. At a higher scale, a noncollagenous XF matrix exists between staggered mineralized collagen fibrils. In general, the XF phase is thought to significantly affect the elastic properties, strength, and toughness of staggered biological structures [1]. The deformations in such structures can be roughly described by two simultaneous mechanisms: stretching of the fibrils and sliding between two adjacent fibrils [2,3]. In fact, finite element simulations indicate that the actual deformations involve both nonuniform stretching of the fibrils and nonuniform stretching and shearing of the XF matrix [4]. In a number of experimental works, the relative stretching of the staggered elements with respect to the overall deformations was measured (e.g., [5,6] in tendon and [7,8] in bone). These works suggest that a significant portion of the overall deformation can be attributed to the XF matrix rather than to the elongation of the staggered elements. The literature includes a wide range of theoretical estimations of the XF modulus, but there are very few experimental data to support these estimations due to the complexity of measuring the modulus of a very soft and thin embedding material.

The relations between the structural characteristics of the staggered array and its elastic properties have been described by a variety of modeling schemes over the past years. Initial mechanical models for stress transfer in a staggered structure were proposed [9,10]. Perturbation approximations have been proposed to evaluate the displacements within a staggered structure, but their accuracy is limited to the particular case of very soft XF material and very thin spacing between the sequential fibrils [11]. A model for a generic staggered geometry, termed here the Bar-On–Wagner (BW) model, was recently formulated [4]. This model provides an approximate analytical solution for the displacement and stress fields, and its accuracy is well supported by finite element simulations for a wide range of staggered configurations.

In the present work, the effect of the XF modulus on the deformations of the fibril (or platelet) elements within a staggered structure is evaluated. Analytical relations are derived from the BW model, and the effect of variations in the XF stiffness is examined. We then use the analysis to back-calculate the yet unmeasured modulus of the XF phase from experimental deformation data, thereby providing a simple alternative to more complex direct measurements. This is illustrated for parallel-fiber bone.

A staggered structure, as typically can be found in bone, tendon, nacre, and more, is considered here as a two-dimensional array of fibrils (or platelets) embedded inside an XF matrix in a staggered periodic manner. The structure is characterized by a repeated unit cell, as shown in Fig. 1. The fibrils and the XF matrix are assumed to be well-bonded and isotropic, with Young moduli E_{XF} and E_f

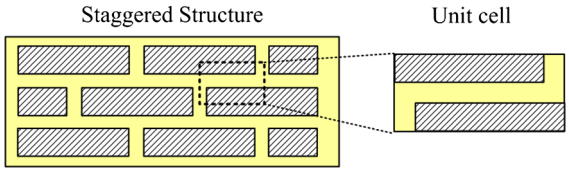

FIG. 1 (color online). A two-dimensional staggered structure and its unit cell.

(for simplicity, we consider $\nu_{XF} = \nu_f = 0.3$). The staggered array can be characterized by three parameters: the fibril volume fraction ϕ_f, aspect ratio ρ_f, and thickness ratio between the fibril and the unit cell Δ_f [12]. If the fibrils' longitudinal and lateral spacings are considered to be equal, the structure can be defined by ϕ_f and ρ_f, where $\Delta_f(\phi_f, \rho_f)$. Upon macroscopic deformation ($\hat{u}$) of the unit cell, both the matrix and the staggered fibrils are being deformed in a nonuniform manner. This elastic response is adequately described by the BW model, providing an analytical expression for the local deformation field and giving a close formula for the overall effective modulus of the staggered array [4]. Figure 2 plots representative deformation functions along the upper fibril within the unit cell, calculated by the BW model for $\phi_f = 0.5$, $\rho_f = 10$, and selected $E^*_{XF} = E_{XF}/E_f$ ratios. The local displacements $u(x)$ are normalized by the overall deformation of the unit cell ($\hat{u}$); u_f marks the displacement at the edge of the fibril, and $\varepsilon_f = u_f/\hat{u}$ represents the deformation ratio between the fibril and the unit cell. In practice, ε_f was measured for different types of biological materials such as tendon [5,6], parallel-fiber bone [7,8], and more. The effective modulus of the staggered structure, E_{eff}, is calculated for each of the selected E^*_{XF} ratios, and the normalized effective modulus $E^*_{\text{eff}} = E_{\text{eff}}/E_f$ is indicated in the figure. The XF matrix in such staggered structures functions as a medium responsible for load transmission between the discontinuous fibrils, modulated by its stiffness. Considering, for example, the curves in Fig. 2, the presence of soft XF material yields relatively mild fibril deformations (low ε_f) and a low overall modulus of the structure, an indication of poor load transmission by the XF medium; stiffer XF materials are associated with improved load transmission, leading to more significant fibril deformations (higher ε_f ratios) and a higher overall modulus.

In general, the fibril deformation ratio (ε_f) is an analytical function of E^*_{XF}, which can be extracted from the BW solution for any specific staggered geometry (i.e., ϕ_f, ρ_f).

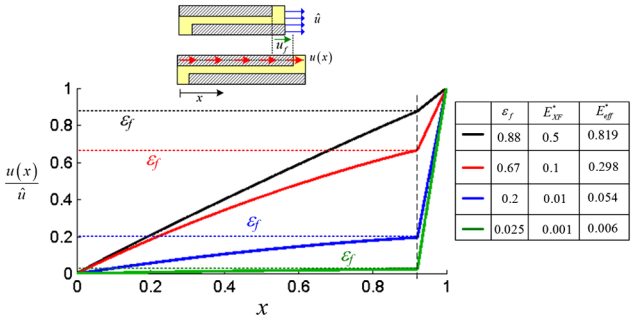

FIG. 2 (color online). The normalized deformation field along the upper region plotted for selected $E^*_{XF} = E_{XF}/E_f$ ratios. $E^*_{\text{eff}} = E_{\text{eff}}/E_f$ is given for each case. The vertical dashed line indicates the edge of the fibril, and the horizontal dotted lines represent $\varepsilon_f = u_f/\hat{u}$.

This function is plotted in Fig. 3 for selected staggered configurations, including different fibril contents ($\phi_f = 0.2, 0.5, 0.7, 0.9, 0.95$) and two aspect ratios: $\rho_f = 100$, which is typical of long fibrous materials such as tendon, bone, and enamel [Fig. 3(a)], and $\rho_f = 10$ representing brick-and-mortar geometry as in nacre [Fig. 3(b)]. The plots are shown on a half-log scale for $10^{-5} < E^*_{XF} < 10^{-2}$, a typical range for most staggered biological materials. Figure 3 shows that the fibril deformation ratio (ε_f) increases as ϕ_f and ρ_f increase—indicating that a greater portion of the load is being sustained by the fibrils resulting in a stiffer structure.

It can be seen that the curves in Fig. 3 exhibit a logarithmiclike dependence (shown by the dashed lines) along part of the E^*_{XF} range:

$$\varepsilon_f = \frac{\log(E^*_{XF}/E^0_{XF})}{\log(E^1_{XF}/E^0_{XF})}, \tag{1}$$

where E^0_{XF} and E^1_{XF} are defined as the intersection point between the approximated logarithmic curve with $\varepsilon_f = 0$ and $\varepsilon_f = 1$, respectively. Both E^0_{XF} and E^1_{XF} are functions of the staggered geometry, and their magnitudes increase as ϕ_f and ρ_f decrease. Within the region $E^0_{XF} < E^*_{XF} < E^1_{XF}$, the elastic deformations of the staggered structure are significantly affected by the XF modulus. In the case of $E^*_{XF} < E^0_{XF}$, the fibril deformations can be considered negligible compared to the overall deformation, and the overall stiffness of the staggered structure is only weakly affected by the modulus of the fibrils, despite the fact

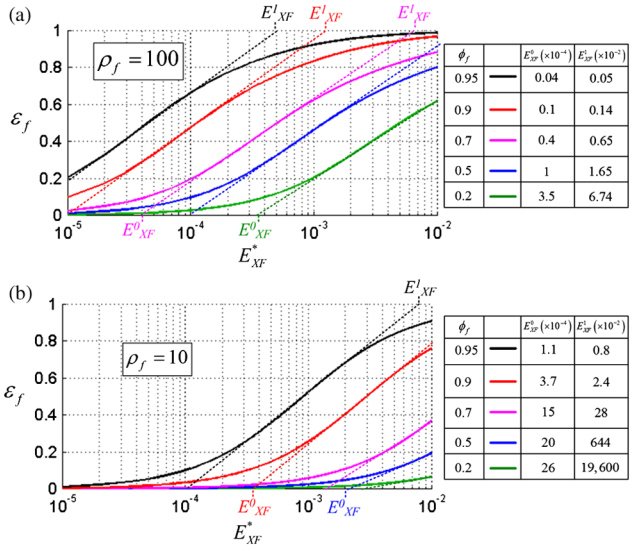

FIG. 3 (color online). ε_f is plotted as a function of E^*_{XF} for (a) $\rho_f = 100$ and (b) $\rho_f = 10$, and varying ϕ_f values. The dashed lines represent semilogarithmic approximations of the curves. E^0_{XF} and E^1_{XF} represent the asymptotic E^*_{XF} values, corresponding to $\varepsilon_f = 0$ (no fibril deformation) and $\varepsilon_f = 1$ (as in parallel fibril geometry), respectively.

that E_f is much greater than E_{XF}. At the other extreme, $E^*_{XF} > E^1_{XF}$ represents an asymptotic case in which the fibril stretching is equal to the overall deformation and the fibrils sustain a major portion of the load (as in the Voigt model). Further enhancement of E^*_{XF} beyond E^1_{XF} only mildly increases the overall modulus of the structure.

Different biological structures include various types of staggered configurations. Nacre and the tooth enamel are examples of stiff and tightly packed configurations, consisting of $E^*_{XF} \approx 10^{-2}$, $\phi_f \approx 0.95$, and $\rho_f \approx 10$ and $\rho_f \approx 100$, respectively [12,13]. According to Figs. 3(a) and 3(b), such configurations are expected to exhibit significant fibril deformations ($\varepsilon_f \approx 0.8$–$0.9$), although no experimental evidence is currently available. Tendon is a more compliant staggered structure, made of long collagen fibrils ($\phi_f \approx 0.9$ and $\rho_f \approx 100$) embedded inside a very soft XF matrix with $E^*_{XF} \approx 10^{-4}$ [14]. Deformation measurements in tendon indicate that $\varepsilon_f \approx 0.43$ [5,6], consistent with the theoretical estimation in Fig. 3(a). Figure 3 can be applied to design synthetic staggered structures, where unique properties can be achieved at the extremes of the E^*_{XF} range. For example, designing toward $E^*_{XF} < E^0_{XF}$ (negligible fibril deformations) results in relatively soft structures with potentially improved fracture resistance due to the presence of the stiff staggered elements. This has been recently demonstrated with carbon nanotube reinforced poly-methylmetacrylate electrospun fibers as well as with bioinspired collagen-HA electrospun fibers, showing that the stiffness of the composite fibers including a small amount of carbon nanotubes or HA is comparable to the "pristine" fibers (without carbon nanotubes or HA), but their strength and toughness are significantly increased [15,16].

Despite the significance of the XF modulus with respect to the elastic response of staggered biological structures, its value has rarely been measured due to experimental complexity. By using the above analysis, we now evaluate the XF modulus by back-calculating it from experimental data of the fibril deformations. The procedure is demonstrated for parallel-fiber bone tissue which includes two scales of staggered elements as presented in Fig. 4. The larger scale of the bone tissue consists of long and tightly packed mineralized collagen fibrils arranged in a staggered manner inside an XF matrix. At the smaller scale, the fibrils themselves are made of staggered HA platelets (denoted by the subscript "p") embedded inside a collagen matrix [8,12]. These HA platelets are typically 60–100 nm long and 2–6 nm thin, and their c axis coincides with the stagger direction [17]. Experimental data for the platelet and fibril deformation ratios [8], defined as $\varepsilon_p = u_p/u_f$ and $\varepsilon_f = u_f/\hat{u}$, are used to evaluate the elastic properties at the different scales of the bone tissue. Subsequently, the modulus of tissue as a whole (E_{tissue}) is calculated, and the analysis is compared with independent experimental data from Refs. [7,8].

First, the modulus of the collagen matrix within the fibril is evaluated from small-scale deformations data, by which

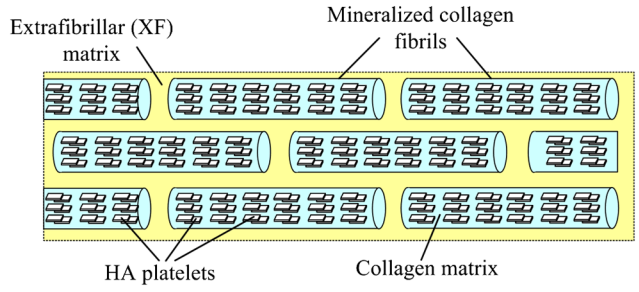

FIG. 4 (color online). A schematic description of parallel-fiber bone tissue viewed as a two-scale staggered structure.

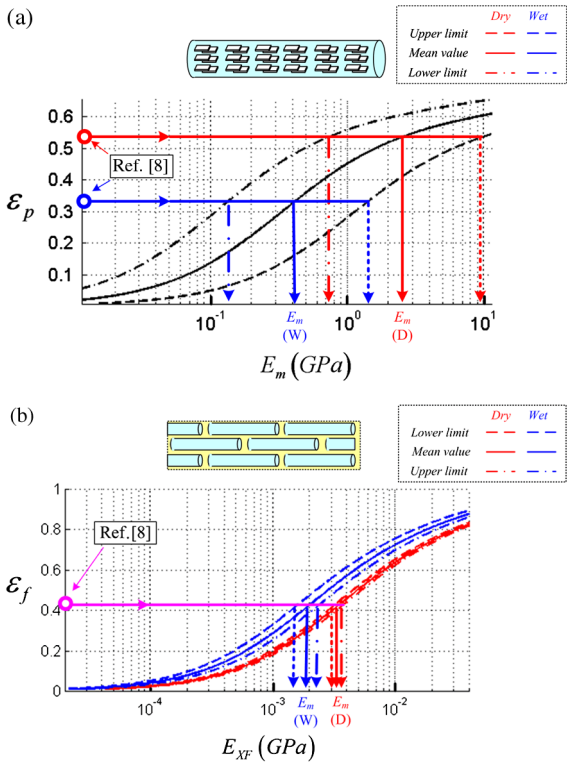

FIG. 5 (color online). (a) The platelet deformation ratio (ε_p) of parallel-fiber bone as a function of the modulus of the collagen matrix (E_m) and the stagger parameters $\phi_p = 0.5 \pm 0.1$, $\rho_p = 30 \pm 10$, and $\Delta_p = 0.7 \pm 0.1$. The red and blue symbols represent the experimentally measured ε_p ratios, and the vertical lines lead to the corresponding E_m values for wet and dry conditions, respectively. The full vertical lines correspond to the mean value E_m, and the dashed vertical lines represent the estimation bounds. (b) The fibril deformation ratio (ε_f), as a function of the modulus of the XF matrix (E_{XF}) and the stagger parameters $\phi_p = 0.5 \pm 0.1$, $\rho_p = 30 \pm 10$, and $\Delta_p = 0.7 \pm 0.1$. The purple symbol represents the experimentally measured ε_f ratio for both wet and dry conditions. The full red and blue vertical lines correspond to the mean value E_{XF}, and the dashed vertical lines represent the estimation bounds.

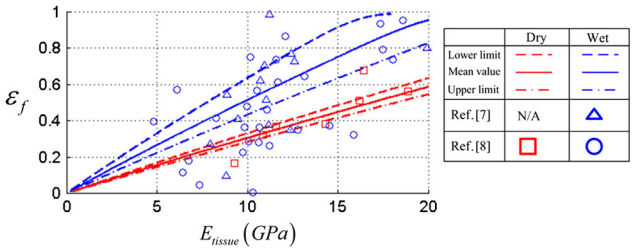

FIG. 6 (color online). ε_f as a function of the overall modulus of the bone tissue (E_{tissue}). The lines represent the proposed theoretical predictions, and the symbols are the experimental data from [7,8]. The red and blue colors correspond to dry and wet conditions, respectively.

the corresponding modulus of the fibril is estimated. The fibril is described as a staggered array with a 67 nm long unit cell [9]. $\phi_p = 0.5 \pm 0.1$, $\rho_p = 30 \pm 10$, and $\Delta_p = 0.7 \pm 0.1$ are considered as relevant stagger parameters, accounting for the variability in platelet dimensions [17]. ε_p is calculated for a range of collagen modulus values (E_m), using $E_p = 114$ GPa as the modulus of the platelet. The results are plotted in Fig. 5(a). Under dry conditions the measured platelet deformation ratio is $\varepsilon_p \approx 0.53$ [8], which corresponds to a mean value of $E_m(\text{dry}) \approx 2.5$ GPa as shown by the full red line in Fig. 5(a). Extreme bounds for the modulus estimations, $0.7\ \text{GPa} < E_m(\text{dry}) < 9\ \text{GPa}$, are indicated by the red dashed lines in Fig. 5(a) and are in agreement with the literature data (e.g., see [8,9,18]). Using the formula proposed in Ref. [12], we find $E_f(\text{dry}) \approx 43.5 \pm 3.5$ GPa, consistent with finite element simulation results [12,13]. Under wet conditions the measured platelet deformation ratio is $\varepsilon_p \approx 0.34$ [8], which reflects a significant softening of the collagen matrix with a mean value of $E_m(\text{wet}) \approx 0.4$ GPa [full blue line in Fig. 5(a)] and an estimation range of $0.1\ \text{GPa} < E_m(\text{wet}) < 1.4\ \text{GPa}$ [blue dashed lines in Fig. 5(a)]. This leads to a more compliant fibril with $E_f(\text{wet}) \approx 25 \pm 5$ GPa.

Next, ε_f is calculated for a range of XF modulus ratios (E_{XF}) by considering $\rho_f = 100$ and $\phi_f = 0.9$ as typical parameters for the staggered fibril array [8,12] and using $E_f(\text{dry})$ and $E_f(\text{wet})$ from the previous section. The results are plotted in Fig. 5(b) for both wet and dry conditions. Note that the resultant curves could also be extracted from Fig. 3(a) by scaling the horizontal axis via $E_{\text{XF}} = E^*_{\text{XF}} E_f$. Following the experimental measurements, $\varepsilon_f \approx 0.41$ for both dry and wet conditions [8], according to which the XF moduli are estimated to be $E_{\text{XF}}(\text{dry}) \approx 3 \times 10^{-3}$–$3.5 \times 10^{-3}$ GPa and $E_{\text{XF}}(\text{wet}) \approx 1.5 \times 10^{-3}$–$2.2 \times 10^{-3}$ GPa, as shown by the dashed lines in Fig. 5(b). Note that, in spite of the fact that both the fibrils and the XF matrix become more compliant in wet conditions, the fibril deformation ratio in parallel-fiber bone (ε_f) remains insensitive to the hydration ratio.

To validate the above fibril and XF moduli estimations, the overall modulus of the tissue is calculated by using the formula in Ref. [12] and compared with independent experimental data from the literature. As an initial validation step, we evaluate the modulus of the tissue by using E_f and E_{XF} from the previous section. This results in $E_{\text{tissue}}(\text{dry}) \approx 13.8 \pm 1$ GPa and $E_{\text{tissue}}(\text{wet}) \approx 8 \pm 1.5$ GPa for the moduli of the dry and wet tissues, respectively, showing a fairly good agreement with the experimental data (see Table 1 in Ref. [8]). Furthermore in Fig. 6, where the data from [8] are normalized, as necessary, by the averaged measured value of ε_p, the theoretical overall modulus of the tissue is calculated for values relevant to the experimental range of ε_f, by repeating the above procedure for both wet and dry conditions. These theoretical estimations are also plotted in Fig. 6, showing good agreement with the experimental data across the entire range of measured ε_f and E_{tissue} values. Figure 6 demonstrates the effectiveness of the back-calculation procedure for evaluating the modulus of the XF matrix from the deformation measurements, as applied here on a rather complex two-scale staggered biological structure.

In conclusion, we have shown that the modulus of the XF matrix is expected to have a significant effect on the elastic deformations and the overall stiffness of a staggered structure. We are able to predict this yet unmeasured modulus based on experimentally available deformation data, as demonstrated for parallel-fiber bone tissue.

We acknowledge support from the Israel Science Foundation (Grant No. 1509/10 and from the G. M. J. Schmidt Minerva Centre of Supramolecular Architectures. This research was made possible in part by the generosity of the Harold Perlman family.

*Corresponding author.
Daniel.Wagner@weizmann.ac.il

[1] B. Ji and H. Gao, Annu. Rev. Mater. Res. **40**, 77 (2010).
[2] N. Sasaki and S. Odajima, J. Biomech. **29**, 1131 (1996).
[3] J. E. Scott, J. Physiol. **553**, 335 (2003).
[4] B. Bar-On and H. D. Wagner, J. Mech. Phys. Solids **59**, 1685 (2011).
[5] P. Fratzl, K. Misofa, I. Zizak, G. Rapp, H. Amenitsch, and S. Bernstorff, J. Struct. Biol. **122**, 119 (1998).
[6] H. R. C. Screen, D. L. Bader, D. A. Lee, and J. C. Shelton, Strain **40**, 157 (2004).
[7] H. S. Gupta, W. Wagermaier, G. A. Zickler, D. Raz-Ben Aroush, S. S. Funari, P. Roschger, H. D. Wagner, and P. Fratzl, Nano Lett. **5**, 2108 (2005).
[8] H. S. Gupta, J. Seto, W. Wagermaier, P. Zaslansky, P. Boesecke, and P. Fratzl, Proc. Natl. Acad. Sci. U.S.A. **103**, 17 741 (2006).
[9] I. Jager and P. Fratzl, Biophys. J. **79**, 1737 (2000).
[10] B. Ji and H. Gao, J. Mech. Phys. Solids **52**, 1963 (2004).
[11] G. Liu, B. Ji, K.-C. Hwang, and B. Cheong Khoo, Compos. Sci. Technol. **71**, 1190 (2011).

[12] B. Bar-On and H. D. Wagner, J. Biomech. **45**, 672 (2012).
[13] B. Bar-On and H. D. Wagner, J. Mech. Behav. Biomed. Mater. **12**, 174 (2012).
[14] C. J. Hooley and R. E. Chohen, Int. J. Biol. Macromol. **1**, 123 (1979).
[15] X.-M. Sui and H. D. Wagner, Nano Lett. **9**, 1423 (2009).
[16] J. Ji, B. Bar-On, and H. D. Wagner, J. Mech. Behav. Biomed. Mater. (to be published).
[17] E. Beniash, Nanomed. Nanobiotech. **3**, 47 (2011).
[18] U. Akiva, H. D. Wagner, and S. Weiner, J. Mater. Sci. **33**, 1497 (1998).